Multilayer Networks with Higher-order Interaction Reveal the Impact of Collective Behavior on Epidemic Dynamics

I. Introduction

In the absence of pharmaceutical interventions, situational awareness and collective adoption of protective behaviors are pivotal to combat spreadout of infectious diseases, as demonstrated by the ongoing COVID-19 pandemic and the flare-up or resurgent outbreaks around the world. The integration of awareness into mathematical models, mainly through variants of susceptible-infectious-recovered (SIR) models, has been widely investigated since the onset of COVID-19 [1]. Most of these models merely capture oversimplified behaviors (e.g., social distancing or not) and fail to capture the sophisticated mechanisms underlying behavioral responses, including the individual perception of infection risk and bounded rationality, government mandate, socioeconomic cost and fatigue on adherence to containment policies, as well as social influence [2-5]. The interplay between the collective behavioral response of the population and the contagion dynamics has a significant bearing on the epidemic evolution.

Game-theoretic models explicitly account for behavioral adaptation and the connection with epidemic spreading [6], mostly with a separation of time scales between the spreading dynamics and behavioral response [7-10]. Inspired by [11], we study the coevolution of the spreading dynamics and behavioral adaptation under the same time scale and investigate the decision-making process under the influence of risk perception, behavioral change costs, compliance fatigue, social influence, as well as bounded rationality [12]. As behavior dynamics has been recognized as one driving force behind resurgent outbreaks of COVID-19, there is a pressing demand for a paradigm shift from purely rational and reactive behavior modeling to a more comprehensive response

computational framework that can predict the epidemic evolution and provide guidance on intervention policy design.

Network models have been widely deployed to describe agent interactions. For instance, a single-layer network was suggested in [13] to incorporate agent behavior to extend the conventional susceptible-exposed-infectious-recovered (SEIR) model. The decision of each agent to take a certain behavioral response is modeled via an evolutionary game model, considering the underlying cost. Ye *et al.* [11] instead suggested a two-layer network to study the interplay between agent behavior from a social layer and the spreading dynamics on a physical layer. Particularly, as we have observed during the COVID-19 pandemic, social media play a vital role in reshaping our perception towards the risk of infection and in transforming behavioral responses. Nonetheless, in most existing works, it is assumed that the infectious population resides in the same physical community. It has been reported that contact patterns of residents in one region could be substantially affected by the policies and behavioral responses in other distant regions [14]. Or in other words, we imitate behavioral responses of our social contacts even if we are located in distant communities. Such a "spillover" effect could crimp the effectiveness of intervention policies, and it has not been systematically investigated. On the other hand, numerous behavioral models [6], [15-16] have been proposed to quantify how human behaviors adapt and affect the transmission of contagious diseases assuming pairwise interactions between agents. It is noted, however, that this pairwise interaction assumption may fail to represent more realistic behavioral responses [17]. Instead, a higher-order interaction among the population has been suggested for behavioral adaptation on social networks. Recent studies also underscore that the presence of higher-order interactions substantially sways the dynamics of networked systems, from diffusion and

synchronization to social and evolutionary processes, possibly leading to the emergence of sophisticated collective phenomena [17-19].

To account for such phenomena, we propose a three-layer network platform to study the interplay between behavioral response and contagion process in two distant communities. These two communities interact via a common social network. A simplicial complex is adopted to model the high-order interactions on the social layer, and a game-theoretic model is then utilized to elucidate the behavioral change of agents. This theoretic model could help harvest policy-relevant insights into the course of contagion spreading dynamics.

It is noteworthy to highlight that our model is not intended to replicate real curves because we are more interested in specific system reactions, such as behavioral responses and changes. Generally, most results caused by diverse behaviors are inadequate data to characterize behaviors. If we fully focus on the result and ignore the mechanisms underlying these behaviors, the result will no longer be precise when the behavioral responses are changed. Currently, most COVID-19 predictions are inaccuracy and their prediction curve are too smooth to be true because the practical curves are oscillations. Thus, we do not target reproducing real results or curves but focus on analytical insights. (For a more in-depth look, you can find the proposed model and numerical findings in the appendix.)

II. Findings and discussion

In this study, we build a 3-layer network to inspect the interplay between two isolated physical communities via a common social-influence layer, and articulate the coevolution of behavioral changes of the agents and spreading dynamics of epidemics. A game-theoretic model is developed to capture the coupled behavior-disease dynamics, subject to measures that mimic the impact of government intervention policy, risk perception, compliance cost, and imitation of social contact's

behaviors. To avoid a simplistic pairwise interaction formulation, we employ a framework that allows for high-order social interactions in the form of simplicial complexes. Results suggest that the simplicial complex setting for the interaction among the agents enhances the risk-averse or risk-taking behaviors, depending on the contact's response to the social influence (see Fig. 5 in appendix). Moreover, the conventional SEIR model generally miscalculates the infection case count, since the public may possess different perception on the infection risk and adherence to the government mandate.

Furthermore, as social networks are becoming key avenues for information and opinion formation, particularly during periods of low physical interactions, behavioral adaptation due to social influence has become one critical component to account for in modeling epidemics. This also suggests that policymakers should carefully deal with misinformation and disinformation in a timely manner. Notably, the flareup or resurgent outbreaks of COVID-19 around the world imply that the patchwork intervention policy does not work as anticipated, partially owing to lack of compliance and behavior imitation from social contacts who may reside in a remote community. Thus, coordinated intervention is anticipated to improve the effectiveness of control and mitigation policies. In this sense, our multi-layer network model provides a more sophisticated framework to study this phenomenon, and the insight gleaned therefrom can be adopted to guide policy design for future pandemics, once the model is properly parameterized—which was not an objective of this study.

Reference

[1] D. Wang, M. Small, and Y. Zhao, "Exploring the optimal network topology for spreading dynamics," Phys. Stat. Mech. Its Appl., vol. 564, p. 125535, Feb. 2021, doi: 10.1016/j.physa.2020.125535.

[2] Y.-C. Chen, P.-E. Lu, C.-S. Chang, and T.-H. Liu, "A time-dependent SIR model for covid-19 with undetectable infected persons," IEEE Trans. Netw. Sci. Eng., vol. 7, no. 4, pp. 3279–3294, 2020, doi: 10.1109/TNSE.2020.3024723.
[3] G. C. Calafiore, C. Novara, and C. Possieri, "A modified SIR model for the covid-19 contagion in italy," in 2020 59th IEEE Conference on Decision and Control (CDC), 2020, pp. 3889–3894. doi: 10.1109/CDC42340.2020.9304142.
[4] I. Cooper, A. Mondal, and C. G. Antonopoulos, "A SIR model assumption for the spread of COVID-19 in different communities," Chaos Solitons Fractals, vol. 139, p. 110057, Oct. 2020, doi: 10.1016/j.chaos.2020.110057.
[5] Z. Liao, P. Lan, Z. Liao, Y. Zhang, and S. Liu, "TW-SIR: time-window based SIR for COVID-19 forecasts," Sci. Rep., vol. 10, no. 1, p. 22454, Dec. 2020, doi: 10.1038/s41598-020-80007-8.
[6] A. Rizzo, M. Frasca, and M. Porfiri, "Effect of individual behavior on epidemic spreading in activity-driven networks," Phys. Rev. E, vol. 90, no. 4, p. 042801, Oct. 2014, doi: 10.1103/PhysRevE.90.042801.
[7] P. Poletti, B. Caprile, M. Ajelli, A. Pugliese, and S. Merler, "Spontaneous behavioural changes in response to epidemics," J. Theor. Biol., vol. 260, no. 1, pp. 31–40, Sep. 2009, doi: 10.1016/j.jtbi.2009.04.029.
[8] A. Vespignani, "Modelling dynamical processes in complex socio-technical systems," Nat. Phys., vol. 8, no. 1, Art. no. 1, Jan. 2012, doi: 10.1038/nphys2160.
[9] I. Belykh, M. Di Bernardo, J. Kurths, and M. Porfiri, "Evolving dynamical networks," Phys. Nonlinear Phenom., vol. 267, pp. 1–6, Jan. 2014, doi: 10.1016/j.physd.2013.10.008.
[10] N. Perra, B. Gonçalves, R. Pastor-Satorras, and A. Vespignani, "Activity driven modeling of time varying networks," Sci. Rep., vol. 2, no. 1, Art. no. 1, Jun. 2012, doi: 10.1038/srep00469.
[11] M. Ye, L. Zino, A. Rizzo, and M. Cao, "Game-theoretic modeling of collective decision making during epidemics," Phys. Rev. E, vol. 104, no. 2, p. 024314, Aug. 2021, doi: 10.1103/PhysRevE.104.024314.
[12] H. A. Simon, "Bounded rationality in social science: Today and tomorrow," Mind Soc., vol. 1, no. 1, pp. 25–39, Mar. 2000, doi: 10.1007/BF02512227.
[13] K. M. A. Kabir and J. Tanimoto, "Evolutionary game theory modelling to represent the behavioural dynamics of economic shutdowns and shield immunity in the COVID-19 pandemic," R. Soc. Open Sci., vol. 7, no. 9, p. 201095, doi: 10.1098/rsos.201095.
[14] D. Holtz et al., "Interdependence and the cost of uncoordinated responses to COVID-19," Proc. Natl. Acad. Sci., vol. 117, no. 33, pp. 19837–19843, Aug. 2020, doi: 10.1073/pnas.2009522117.
[15] C. Granell, S. Gómez, and A. Arenas, "Dynamical interplay between awareness and epidemic spreading in multiplex networks," Phys. Rev. Lett., vol. 111, no. 12, p. 128701, Sep. 2013, doi: 10.1103/PhysRevLett.111.128701.
[16] Z. Wang, M. A. Andrews, Z.-X. Wu, L. Wang, and C. T. Bauch, "Coupled disease–behavior dynamics on complex networks: A review," Phys. Life Rev., vol. 15, pp. 1–29, Dec. 2015, doi: 10.1016/j.plrev.2015.07.006.
[17] I. Iacopini, G. Petri, A. Barrat, and V. Latora, "Simplicial models of social contagion," Nat. Commun., vol. 10, no. 1, p. 2485, Dec. 2019, doi: 10.1038/s41467-019-10431-6.
[18] D. Guilbeault, J. Becker, and D. Centola, "Complex contagions: a decade in review," in Complex Spreading Phenomena in Social Systems, S. Lehmann and Y.-Y. Ahn, Eds. Cham: Springer International Publishing, 2018, pp. 3–25. doi: 10.1007/978-3-319-77332-2_1.

[19] D. Wang, Y. Zhao, H. Leng, and M. Small, "A social communication model based on simplicial complexes," Phys. Lett. A, vol. 384, no. 35, p. 126895, Dec. 2020, doi: 10.1016/j.physleta.2020.126895.

Appendix

Model

We present a multilayer network platform to elucidate how the collective behavior of individual agents affects the contagion dynamics on disjoint physical communities. This platform comprises two physical layers that represent two isolated communities A and B, on top of which a networked SEIR model is implemented to capture the disease spreading dynamics. Here, for simplicity, we construct the communities A and B as Barabási-Albert (BA) networks, since many realistic networks follow the preferential attachment principle [1]. The physical networks of communities A and B have N_a and N_b nodes or agents, respectively. In essence, starting with an initial network G_0 of N_0 connected nodes, new nodes are attached to $m < N_0$ original ones to form new edges according to the preferential attachment principle, i.e., with a probability proportional to the degree of existing nodes.

Agents from both communities A and B collectively define a social community C that accommodates social interactions, thus the size $N_c = N_a + N_b$, which indicates that every agent cannot travel between two physical communities A and B (see Fig. 1). These two physical layers have time-varying undirected links, which symbolize the physical contacts or the avenue for disease transmission [2]. Each agent adjusts their risk-taking or risk-averse behaviors as they parse information regarding the global prevalence of the contagion and the response of their neighbors on the social layer. Therefore, the two distant communities could still affect each other regarding

the spreading dynamics indirectly via the social network, even without human mobility in between. This mimics how we perceive information from social media and adapt our behaviors accordingly.

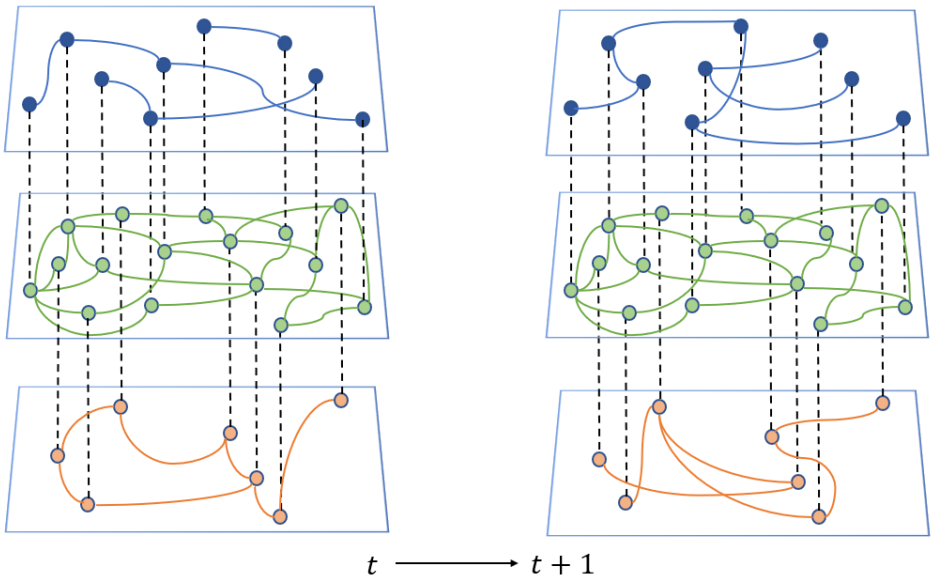

Fig. 1 Illustration of the 3-layer network platform as time evolves: the upper/blue layer and lower/orange layer represent the two physical contact networks or communities *A* and B; the middle/green layer represents the social influence network

We define two utility functions π_a^i and π_r^i to characterize the payoff for risk-averse and risk-taking behaviors of agent i, which hinges on the effective intervention policy $\delta(t)$, imitation of social influence $\omega_i(t)$, compliance cost $\varepsilon_i(t)$ (e.g., economic cost, mental stress, and physical fatigue), and the community's risk perception $\eta(t)$ [3].

$$\pi_a^i(t) = \omega_i(t) + \eta(t) - \varepsilon_i(t) \tag{1a}$$

$$\pi_r^i(t) = -\delta(t) - \omega_i(t) \tag{1b}$$

With a large π_a^i, agent i has a strong sense of situational awareness and tends to be risk-averse, disregarding the effective intervention policy δ. It is further assumed that conservative agents are sensitive to risk perception $\eta(t)$ and compliance cost $\varepsilon_i(t)$, as displayed in Eq. (1a). Conversely, a large π_r^i indicates that agent i is risk-prone. The risk-taking agents generally ignore the risk

perception $\eta(t)$ and compliance cost $\varepsilon_i(t)$. They instead subject their behaviors to government regulations. $\omega_i(t)$ prescribes the social influence on agent i resulting from imitating the behaviors of social contacts. Positive $\omega_i(t)$ indicates imitation of protective behaviors from neighbors, thus boosting $\pi_a^i(t)$; negative $\omega_i(t)$ implies imitation of risk-taking responses, elevating $\pi_r^i(t)$. Following this, we construct a Markov model to characterize the time-dependent behavioral adaption via behavior quotient (BQ) $x_i(t+1)$ of agent i at time stamp $t+1$ with bounded rationality assumption:

$$x_i(t+1) = \frac{e^{\sigma\pi_a^i(t)} - e^{\sigma\pi_r^i(t)}}{e^{\sigma\pi_a^i(t)} + e^{\sigma\pi_r^i(t)}}, \tag{2}$$

where $\sigma > 0$ is a rational scale in the decision-making process. A finite constant σ is assumed for all agents with bounded rationality. As a side note, the two extreme cases of $\sigma \to \infty$ and $\sigma = 0$ indicate fully rational and fully irrational behaviors, respectively. The BQ $x_i(t) \in (-1,1)$ is a continuous variable capturing the effective behavioral response of agent i: if $x_i(t) > 0$, agent i avoids risk and takes protective behavior; for $x_i(t) = 0$, agent i is risk-neutral; if $x_i(t) < 0$, risky behavior is in favor, which could potentially boost the probability of infection. It is noteworthy that the formulation of BQ $x_i(t)$ is a significant departure from the model proposed in [3], in that each agent mimics both risk-averse and risk-taking behaviors. The public weighs the trade-off to adjust their behavioral response, considering the behavior of their social contacts, risk perception, government intervention policy, and compliance cost.

A. Imitation of social behavior

On the social influence layer, we define an imitation function $\omega_i(t)$ to characterize how agent i imitates the behaviors of their social contacts. The simplicial complex has been extensively used to reveal such higher-order interactions: the behavioral imitation occurs with nonlinear

reinforcement characterized by the simplex dimension, rather than bilinearly depending on the number of connecting nodes and their behaviors. Formally, a simplex of dimension d or d-simplex is a collection of $d+1$ vertices $\sigma_d = [j_0, j_1, \dots, j_d]$, and any subset $\sigma_{d'}$ ($d' \leq d$) of σ_d is its sub-simplex or d'-face [4]. That said, σ_d subsumes all subset simplices of dimension $d-1$, and so on recursively. The vertices are called 0-simplices, the edges the 1-simplices and the full triangles the 2-simplices. The collection of simplices and all the sub-simplices or faces defines a simplicial complex. As illustrated in Fig. 2 (b), the agent i (the orange node) interacts with a set of social contacts j_1, j_2 and j_3 via a simplicial 2-simplex, which contains a 1-simplex (e.g., pairwise link of $[i, j_1]$) and a 2-simplex (the full triangle $[i, j_2, j_3]$). Conversely, Fig. 2 (a) illustrates a simplicial 1-complex with only the pairwise interactions. The imitation of social behavior, indexed by ω_i, is induced on the simplicial complex. For computational easiness, we only consider the simplicial complex up to dimension 3 in this study.

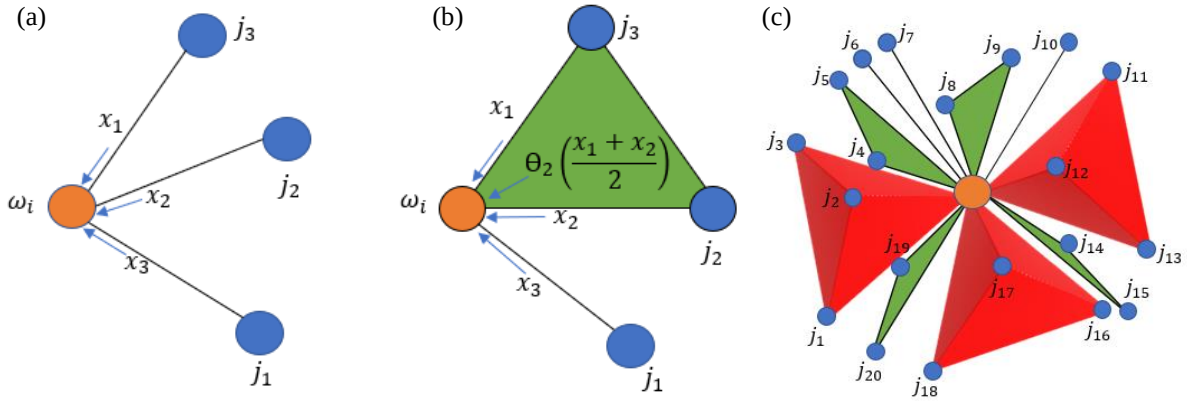

Fig. 2 Illustration of different interactions in the network for agent i (the orange): (a) only pairwise interactions; (b) simplical 2-complex, including the pairwise and full-triangle interactions; (c) a simplicial 3-complex with three 3-simplices (red tetrahedron), four 2-simplices (green triangle), and three 1-simplices.

The enhancement effect for collective interaction of a d'-simplex is given as $\theta_{d'} = (1+\rho_{d'})^{\lambda_{d'}}$, where $\rho_{d'}$ is the proportion of number counts of d'-simplices in the simplicial 3-complex. $\lambda_{d'} =$

$\binom{d'+1}{3}$ underscores the influence of high-order interactions. $\lambda_{d'} = 0$ for $d' < 2$, $\lambda_2 = \binom{2+1}{3} = 1$, and $\lambda_3 = \binom{3+1}{3} = 4$. In the illustrative example depicted in Fig. 2 (c), a simplicial 3-complex contains three 1-simplices, four 2-simplices, and three 3-simplices, thus $\rho_1 = \rho_3 = \frac{3}{10}$, $\rho_2 = \frac{4}{10}$. Correspondingly, the enhancement coefficient for pairwise interaction is fixed as $\theta_1 = 1$ with $\lambda_1 = 0$. Therefore, the imitation of social behavior function for agent i at time t can be represented as:

$$\omega_i(t) = \xi \frac{\theta_1 \sum_{v=1}^{n_{i1}} \bar{x}_v^1 + \theta_2 \sum_{v=1}^{n_{i2}} \bar{x}_v^2 + \theta_3 \sum_{v=1}^{n_{i3}} \bar{x}_v^3}{n_i}, \tag{3}$$

where ξ is the imitation factor that scales the influence of imitation behavior in utility functions π_a^i and π_r^i, n_{i1} is the number of 1-faces, n_{i2} is the number of 2-faces, and n_{i3} is the number of 3-faces associated with agent i. Variables $\bar{x}_v^1$, $\bar{x}_v^2$, and $\bar{x}_v^3$ represent the average BQ of the v^{th}face with orders 1, 2, and 3 respectively. The 1-face is included not only in the 1-simplex but also in the 2-simplex and 3-simplex. Each 1-face contains one neighboring agent for agent i with the average BQ $\bar{x}_v^1(t)$. Here $\bar{x}_v^1(t) = x_{j_v}(t)$, $v = 1, \dots, n_{i1} = 20$ as shown in Fig. 2 (c). Similarly, the 2-face is included not only in the 2-simplex but also in the 3-simplex, and 2-face contains two neighboring agents with average BQ $\bar{x}_v^2(t)$. There are thirteen 2-faces for agent i in Fig. 2 (c), which are $\bar{x}_1^2(t) = \frac{x_{j_1}(t)+x_{j_2}(t)}{2}$, $\bar{x}_2^2(t) = \frac{x_{j_1}(t)+x_{j_3}(t)}{2}$, $\bar{x}_3^2(t) = \frac{x_{j_2}(t)+x_{j_3}(t)}{2}$, $\bar{x}_4^2(t) = \frac{x_{j_4}(t)+x_{j_5}(t)}{2}$, $\bar{x}_5^2(t) = \frac{x_{j_8}(t)+x_{j_9}(t)}{2}$, $\bar{x}_6^2(t) = \frac{x_{j_{11}}(t)+x_{j_{12}}(t)}{2}$, $\bar{x}_7^2(t) = \frac{x_{j_{11}}(t)+x_{j_{13}}(t)}{2}$, $\bar{x}_8^2(t) = \frac{x_{j_{12}}(t)+x_{j_{13}}(t)}{2}$, $\bar{x}_9^2(t) = \frac{x_{j_{14}}(t)+x_{j_{15}}(t)}{2}$, $\bar{x}_{10}^2(t) = \frac{x_{j_{16}}(t)+x_{j_{17}}(t)}{2}$, $\bar{x}_{11}^2(t) = \frac{x_{j_{16}}(t)+x_{j_{18}}(t)}{2}$, $\bar{x}_{12}^2(t) = \frac{x_{j_{17}}(t)+x_{j_{18}}(t)}{2}$, and $\bar{x}_{13}^2(t) = \frac{x_{j_{19}}(t)+x_{j_{20}}(t)}{2}$. Lastly, the 3-face is only included in the 3-simplex, and there are three

3-faces in the illustrative example in Fig. 2 (c). The average BQ $\bar{x}_1^3(t) = \frac{x_{j_1}(t)+x_{j_2}(t)+x_{j_3}(t)}{3}$, $\bar{x}_2^3(t) = \frac{x_{j_{11}}(t)+x_{j_{12}}(t)+x_{j_{13}}(t)}{3}$, and $\bar{x}_3^3(t) = \frac{x_{j_{16}}(t)+x_{j_{17}}(t)+x_{j_{18}}(t)}{3}$.

B. Risk perception

The risk perception reflects how the public perceives the disease prevalence z, the fraction of the population that is infected (exposed and infectious) [5]. A power function for risk perception, $z(t) \in [0,1]$, has been suggested in [3]:

$$\eta(t) = kz(t)^u, \tag{4}$$

where $k > 0$ is the scaling factor and the risk index $u > 0$ captures the population attitude towards the prevalence or the risk. Since $z \in (0,1)$, $u > 1$ indicates that the population discounts the infection risk, and $u < 1$ implies that the public tends to overrate the underlying risk.

C. Government intervention policies

To contain the spreading of infection, the government enacts non-pharmaceutical interventions, such as social distancing, face mask requirement, and lockdowns. $p(t) > 0$ quantifies the strength of such policies at time t, and the policy is adjusted periodically (e.g., every 10 time steps) for each community according to the average prevalence $\bar{z}(t^*)$ of the previous time interval $T \in [t^* - 10, t^* - 1]$, where $t^* = 10 \times \left\lfloor \frac{t}{10} \right\rfloor$ and $\lfloor \cdot \rfloor$ is a floor function. Remarkably, public compliance with social restrictions diminishes as fatigue sets in. To account for the "lockdown fatigue", a fatigue function $\psi(t) = e^{-\left(\frac{t}{\mu}\right)}$ is introduced to portray the diminishing public compliance to the intervention policy as time elapses, regulated by the complying factor μ. Thus, the effective intervention policy δ is given as:

$$\delta(t) = \psi(t)p(t)\,, \tag{5a}$$

$$p(t) = \begin{cases} 0.8, & \bar{z}(t^*) > 0.1 \\ 0.5, & 0.05 \leq \bar{z}(t^*) \leq 0.1 \\ 0.3, & 0.03 \leq \bar{z}(t^*) < 0.1 \\ 0.0, & \bar{z}(t^*) < 0.03 \end{cases}, \quad (5b)$$

Here, the values of $p(t)$ are set arbitrarily, and we do not seek to find the optimal intervention policy. Different evolution trajectory of the infection of the two different communities causes different intervention policies $p(t)$, as shown in Eq. 5 (b). We name this as an adjustable policy, in comparison to the rigid policy to be discussed in section **Numerical result**.

D. Compliance cost

Studies on historical contagion indicates that adherence to government mandate is crucial to slowing the spread of the pandemic [6]. The compliance cost $\varepsilon_i(t)$ symbolizes the cost of abiding by government policies, and it hinders the agent from taking protective behaviors (e.g., shelter-at-home and wearing face masks). The compliance cost $\varepsilon_i(t)$ comprises two components: the immediate cost $c \geq 0$, e.g., basic sanitization cost and psychological frustration, and cumulative protective cost.

$$\varepsilon_i(t) = c + \sum_{\tau=1}^{t} a^{t-\tau} \left(\varphi[x_i(\tau) - 0.2]^+\right) \quad (6)$$

$a \in [0, 1]$ is the cumulative factor representing how the past protective behaviors affect the current compliance cost. As agents respond to the infection in a different way, the cumulative cost hinges on each BQ $x(t)$. $a = 0$ implies a memoryless protective cost structure, such that the protective action course in the history does not affect the current compliance cost. Cost scaling φ indicates the cost associated with the protective behaviors. $[x_i(\tau) - 0.2]^+ = \max(0, x_i(\tau) - 0.2)$ represents that the BQ less than 0.2 will not incur a cost at time τ.

E. Transition probability

On the two physical contact layers (communities A and B), each agent i is in one of 4 possible states $h_i(t) = \{S, E, I, R\}$ at any time t. The infectious (I) spreads the disease to their susceptible (S) neighbors, who then become exposed (E) with a probability $P(h_i(t+1) = E | h_i(t) = S)$:

$$P(h_i(t+1) = E | h_i(t) = S) = \frac{1-x_i(t)}{2} \times \left(1 - (1-\beta)^{N_i(t)}\right), \quad (7)$$

where β is the infection rate when the susceptible agent i contacts infectious neighbors. $N_i(t)$ is the number of infectious neighbors for agent i at time t, and it is time-varying because of the change of agents' states. The expression $\frac{1-x_i(t)}{2} \in (0,1)$ symbolizes the effective disease transmission, citing variation of BQ $x_i(t)$. When $x_i(t) = 1$, agent i refrains from taking any risk, and $x_i(t) = -1$ implies that agent i completely ignores the infection risk. The exposed (E) transitions to the infectious (I) with a probability $P(h_i(t) = I | h_i(t_E) = E)$:

$$P(h_i(t) = I | h_i(t_E) = E) = 1 - e^{-\alpha(t-t_E)}, \quad (8)$$

where t_E is the time at which agent i became exposed (E). This transition occurs at an exponential rate α, or equivalently with an average latent period of $1/\alpha$. In a similar vein, the infectious (I) recovers with a probability $P(h_i(t) = R | h_i(t_I) = I)$:

$$P(h_i(t) = R | h_i(t_I) = I) = 1 - e^{-\gamma(t-t_I)}, \quad (9)$$

where t_I is the time at which agent i becomes infectious (I). The recovery process occurs at an exponential rate γ, or equivalently with an average recovery period of $1/\gamma$.

Numerical results

We utilize the Facebook social network dataset from Network Repository (NR) [7] for the social influence layer, which includes 10004 individual Facebook users or nodes. We construct a simplicial 3-complex for each agent at each time t by randomly selecting a different number of

neighbors (from 1 to 3) to formulate different order simplices. We generate an Erdös-Rényi (ER) random network as the initial network G_0 with size $N_0 = 1000$ and the probability of node connection $C_0 = 0.1$ to construct two BA networks to represent the communities A (the first physical contact layer in our multilayer network) and B (the second physical contact layer) of equal size $N_a = N_b = 5002$ but with disparate density of links. The densely connected network symbolizes the urban area, denoted as community A: each of the new coming nodes will connect to $m_a = 250$ nodes to extend the initial network. The sparsely connected network is analogous to the rural area, denoted as community B: each new coming node will be connected to only $m_b = 50$ existing nodes. The connectivity of these two BA networks represents the maximal physical contacts for each agent throughout the epidemic process. As time evolves, a random set of edges from this connectivity will be chosen for each agent to form the time-varying network. This does not preclude other temporal formation mechanisms [3]. We stress that whereas some epidemic models can reproduce key features of the spreading dynamics, the abundance of mutually incompatible models suggest that there is still substantial uncertainty in data collection and model parameterization, as well as a lack of fundamental understanding of the observed spatiotemporal dynamics [8]. Thus, we do not aim to replicate the infection curve in any particular regions. Rather, we parameterize the model to reveal the general impact of the social interplay on the infection dynamics.

We implement the SEIR compartment model previously described on the two physical layers (the communities A and B), which possess the same key parameters for the COVID-19 pandemic, including the transmission probability per contact β, the incubation rate α, and the recovery rate γ. According to recent studies of COVID-19 [49-50], we set $\beta = 0.06$, $\alpha = 1/7$ and $\gamma = 1/21$. That is to said, we set the incubation period to 7 days and the recovery time to 21 days. To start

with, we randomly assign a 1% of the population for communities A and B to the infectious compartment, and initialize the BQ $x(0) = 0$ and the effective intervention policy $\delta(0) = 0$ for all agents. Disregarding the social influence and behavioral response, the contagion dynamics for the densely-connected urban community A and the sparsely-connected rural community B regulated by the conventional SEIR are showcased in Fig. 3: community A reaches a higher peak infection rate with an earlier arrival time. Nonetheless, there is a far cry between the reality and those curves in Fig. 3: ebbs and flows of COVID-19 case count have been reported globally, and multiple resurgent outbreaks are also observed in the U.S.

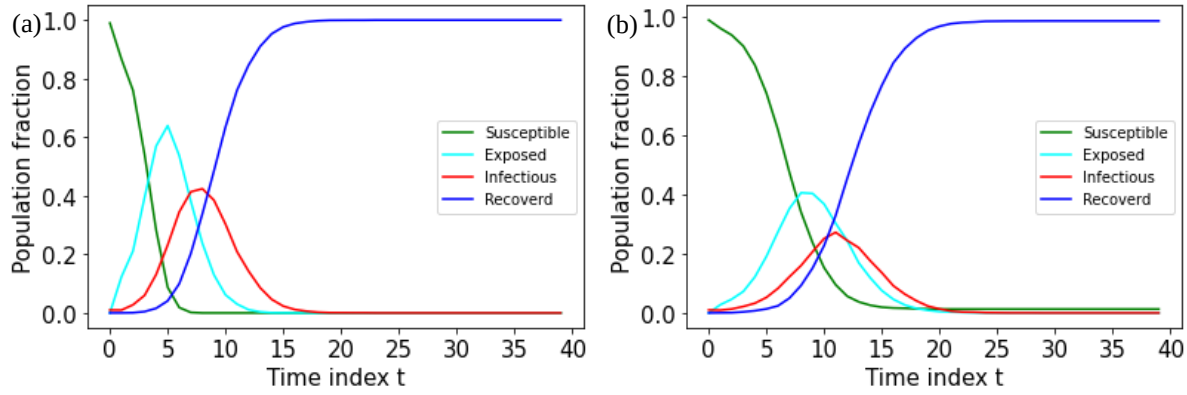

Fig. 3 Population fraction of each compartment under the conventional network SEIR model for (a) communities A and (b) community B, respectively.

A. Spreading dynamics under different risk perceptions

We set the model parameters on the social layer so as to have immediate cost $c = 0.1$, accumulative factor $a = 0.4$, cost scaling $\varphi = 0.7$, imitation factor $\xi = 0.2$, rational rate $\sigma = 10$, and complying factor $\mu = 50$. We initialize the BQ $x(0) = 0$ for all agents on the social layer, i.e., they are all risk neutral at the onset of infection. We also assume a scaling factor $k = 2$ and risk index $u = 0.5$ for a high level of situational awareness of the infection. In this scenario, the public tends to take risk-averse behaviors in line with the prevalence rate, and the compartment flow

dynamics are shown in Fig. 4 (a) and (b) for communities A and B, respectively. Compared to the conventional SEIR model, the infectious compartment exhibits oscillatory patterns, and a much lower peak infectious fraction is observed. Conversely, $k = 0.5$ and $u = 4$ are used for a low level of risk awareness. Hence, the public tends to take risky behaviors, resulting in marked increase of the infectious population, as shown in Fig. 4 (c) and (d). Numerically, such risky behaviors lead to BQ $x \to -1$ or $\frac{1-x_i(t)}{2} \to 1$ for most agents at the earlier stage of the contagion. According to Eq. (7), our model is approximately equivalent to the conventional SEIR model in this condition, particularly the first 10 time steps before triggering the intervention policy. Next, the non-pharmaceutical intervention is enacted to suppress the spread of contagion. For community A with high population density, the adjustable intervention is not sufficiently intense to contain the disease spread when the public is averse to safeguard measures, which is distinguishable from the infection curves in Fig. 3 (a) and Fig. 4 (c). For community B, the susceptible levels off rapidly after the policy is enacted, which represents a significant departure from the curve in Fig. 3 (b).

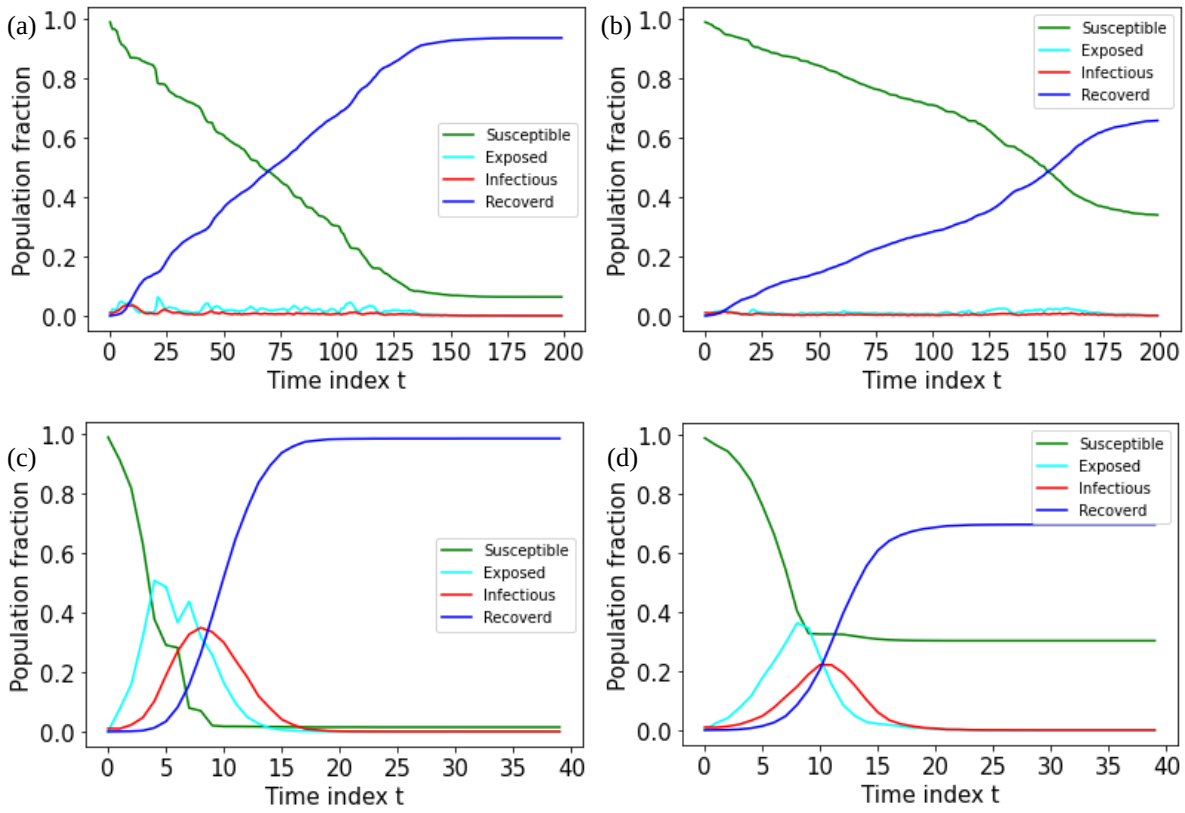

Fig. 4 Population fraction of each compartment under the proposed game-theoretic network SEIR model for (a) community *A* and (b) community *B* with risk-averse behavioral response, and (c) community *A* and (d) community *B* with risk-taking behavioral response.

At the onset of the pandemic, the prevalence $z(t)$ edges up rapidly. When the public possesses high risk aversion (with $k = 2$ and $u = 0.5$), the risk perception η increases at a faster pace than the compliance cost ε_i, promoting risk-averse behaviors (see Eq. 1 (a)). The imitation of social behaviors further elevates the population BQ, eventually bending the infection curve. The counterbalance between the constituent components of the utility functions is manifested as the spikes on the prevalence curves in Fig. 5 (a) and (b). When the public generally ignores the infection risk with $k = 0.5$ and $u = 4$, the compliance cost ε_i dominates the utility function. The behavior imitation further enhances such risk-prone behaviors. Overall, at this extreme risk ignorance, all agents behave without considering the infection, thus the prevalence is fairly similar

to the conventional SEIR model without behavioral response (see Fig. 5 (c) and (d)). We also note that with high-order interactions between agents, the imitation of social behaviors captures the reinforcement effect. As displayed in Fig. 5 (a) and (b), when the population is on high alert, the prevalence rate curves exhibit a lower peak for both communities A and B under the simplicial complex framework compared to the pairwise interaction. At the low risk perception level, the reinforcement of risky responses leads to elevated peaks for communities A and B, though the difference is not substantial as illustrated in Fig. 5 (c) and (d).

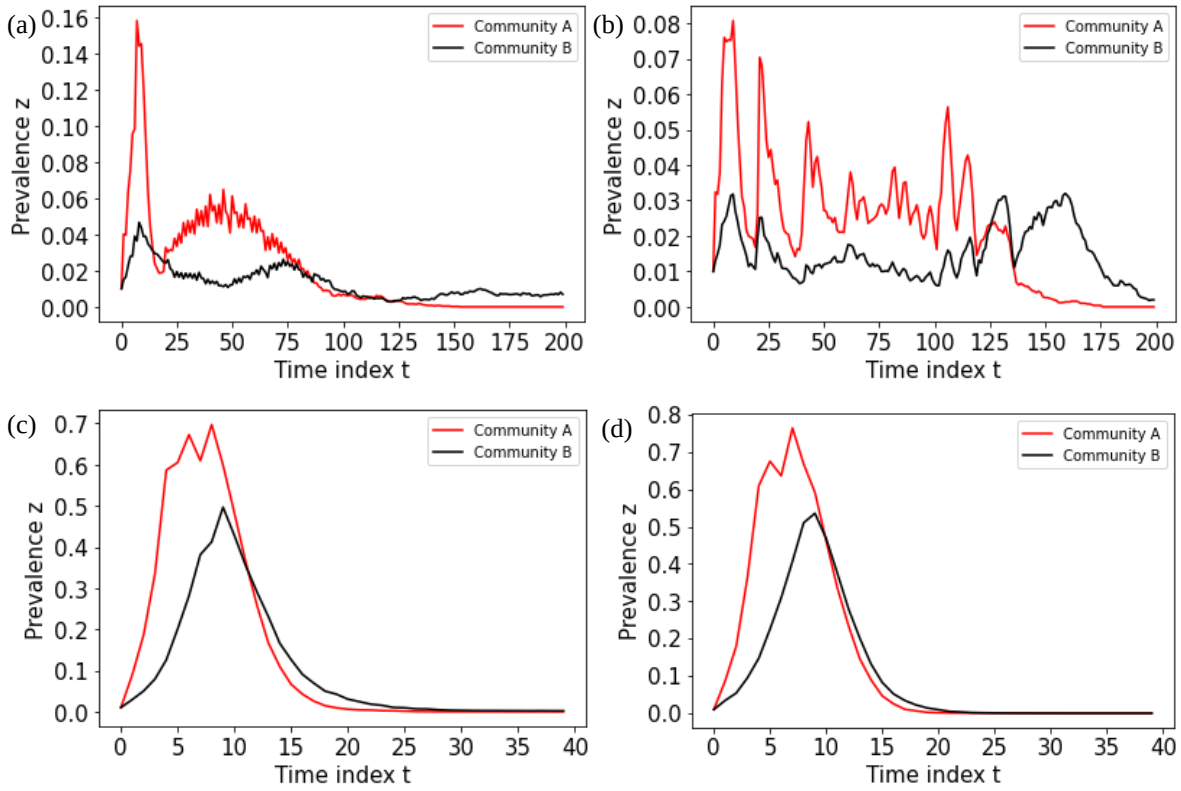

Fig. 5 The prevalence rate $z(t)$ from the game-theoretic network SEIR for the two communities with (a) pairwise and (b) high-order interactions on the social influence layer under risk-averse behavioral response, and with (c) pairwise and (d) high-order interactions on the social influence layer under risk-taking response.

B. The influence of control policy

We conduct another set of simulations to investigate how the control policy in one community affects the other indirectly via the social layer, with 2 levels of intensity, namely, weak $\delta(t) = 0.1$

and strict $\delta(t) = 1.0$ for all time t, instead of the adjustable control policies given in Eq. (5). Here, we only consider the risk averse scenario. First, we apply a strict control policy to community A and maintain the adjustable policy in line with the prevalence rate for community B. As shown in Fig. 6 (a), the bold action against the infection significantly suppresses the prevalence rate for community A, compared to the adjustable policy in Fig. 5 (b). Such a strict policy substantially subdues the utility for risky behaviors, thus promoting conservative responses. Simultaneously, agents in community B imitates the behavior of their social contacts, resulting in fluctuation of the prevalence. As time evolves, with the strict government mandate in place, more and more agents adopt the risk-averse responses, and the prevalence in community B also settles at a low level. Next, we impose a strict control policy on community B and maintain the adjustable policy for community A. As shown in Fig. 6 (b), the strict policy suppresses the prevalence for community B and agents in community A imitate the protective behaviors in community B to also diminish their prevalence as compared to the scenario of adjustable policies for both communities in Fig. 5 (b).

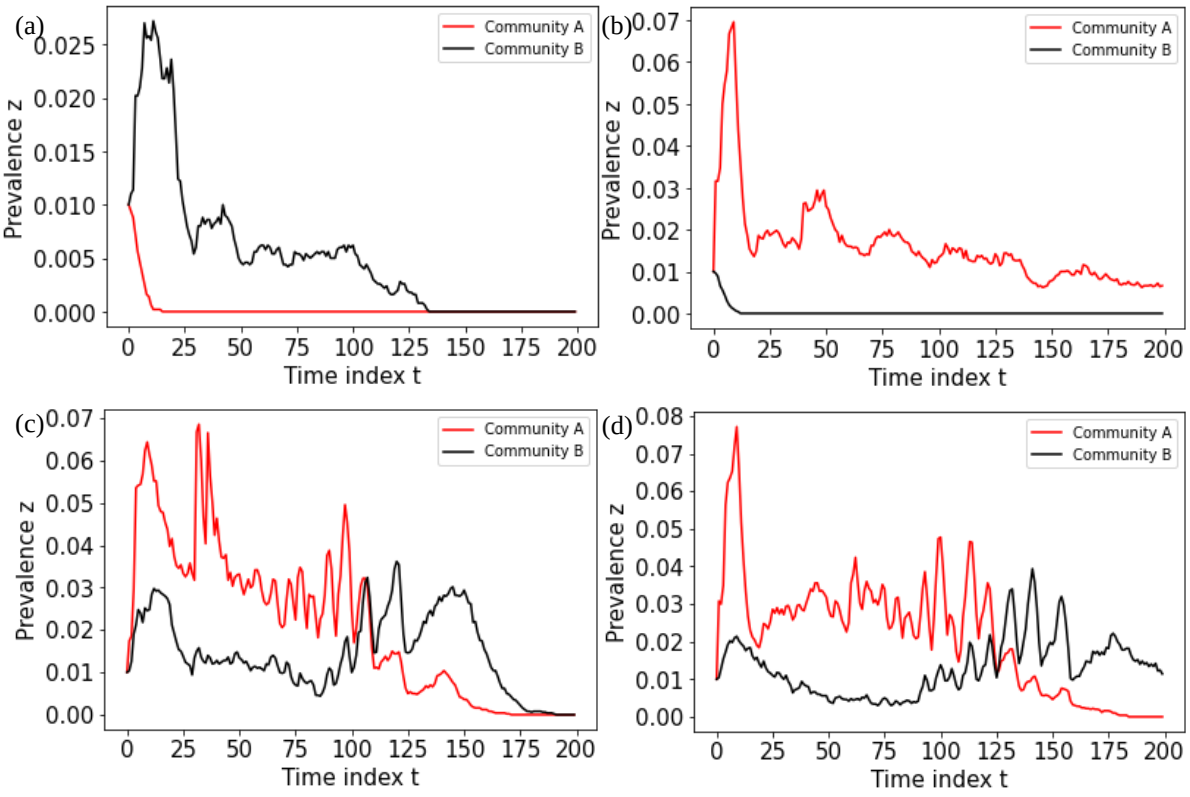

Fig. 6 The prevalence rate $z(t)$ from the game-theoretic network SEIR for the two communities with different levels of control policies: (a) strict control policy $\delta(t) = 1.0$ for community A; (b) strict control policy $\delta(t) = 1.0$ for community B; (c) weak control policy $\delta(t) = 0.1$ for community A; (d) weak control policy $\delta(t) = 0.1$ for community B.

Subsequently, a weak control policy is enacted for one community and an adjustable policy is maintained for another one. As illustrated in Fig. 6 (c) and (d), overall, as the population is risk averse, the weak control policy has only a modest impact on agent behaviors and the prevalence of both communities. Compared to Fig. 5 (b), the prevalence in community A with weak control policy (see Fig. 6 (c)) is slightly decreased in the first 10 time steps, because the adjustable policy is inactive. Likewise, a weak control policy is also imposed on community B leading to a slightly smaller prevalence in community B. It is further noted that the strength of the weak control policy ($\delta(t) = 0.1$) is lower than the active adjustable policy ($\delta(t) \geq 0.3$) in community A but higher than the inactive adjustable policy ($\delta(t) = 0.0$) in community B, as given by the average disease

prevalence in both Fig. 6 (c) and (d). Therefore, the overall prevalence in community A with a weak control policy is higher than the adjustable policy but the overall prevalence rate in community B with a weak control policy is lower than the adjustable policy.

Based on the results of Fig. 6, we conclude that the control policy for one community can have a significant influence on another community due to the imitation of social behavior ω. Thus, it appears that to reduce the prevalence of the pandemic fast, the best way is to impose a strict control policy on the denser population. Conversely, imposing a strict control policy on a lowly dense population community cannot halt the pandemic fast.

Reference

[1] R. Albert and A.-L. Barabási, "Statistical mechanics of complex networks," *Rev. Mod. Phys.*, vol. 74, no. 1, pp. 47–97, Jan. 2002, doi: 10.1103/RevModPhys.74.47.

[2] N. Masuda, J. C. Miller, and P. Holme, "Concurrency measures in the era of temporal network epidemiology: a review," *J. R. Soc. Interface*, vol. 18, no. 179, p. 20210019, doi: 10.1098/rsif.2021.0019.

[3] M. Ye, L. Zino, A. Rizzo, and M. Cao, "Game-theoretic modeling of collective decision making during epidemics," *Phys. Rev. E*, vol. 104, no. 2, p. 024314, Aug. 2021, doi: 10.1103/PhysRevE.104.024314.

[4] I. Iacopini, G. Petri, A. Barrat, and V. Latora, "Simplicial models of social contagion," *Nat. Commun.*, vol. 10, no. 1, p. 2485, Dec. 2019, doi: 10.1038/s41467-019-10431-6.

[5] C. S. McMahan *et al.*, "COVID-19 wastewater epidemiology: a model to estimate infected populations," *Lancet Planet. Health*, vol. 5, no. 12, pp. e874–e881, Dec. 2021, doi: 10.1016/S2542-5196(21)00230-8.

[6] D. Holtz *et al.*, "Interdependence and the cost of uncoordinated responses to COVID-19," *Proc. Natl. Acad. Sci.*, vol. 117, no. 33, pp. 19837–19843, Aug. 2020, doi: 10.1073/pnas.2009522117.

[7] R. A. Rossi and N. K. Ahmed, "The network data repository with interactive graph analytics and visualization," *29th AAAI Conf. Artif. Intell.*, pp. 4292–4293, Jan. 2015.

[8] D. Brockmann and D. Helbing, "The hidden geometry of complex, network-driven contagion phenomena," *Science*, vol. 342, no. 6164, pp. 1337–1342, Dec. 2013, doi: 10.1126/science.1245200.

[9] S. M. Moghadas *et al.*, "The implications of silent transmission for the control of COVID-19 outbreaks," *Proc. Natl. Acad. Sci.*, vol. 117, no. 30, pp. 17513–17515, Jul. 2020, doi: 10.1073/pnas.2008373117.

[10] C. Hou *et al.*, "The effectiveness of quarantine of Wuhan city against the Corona Virus Disease 2019 (COVID-19): A well-mixed SEIR model analysis," *J. Med. Virol.*, vol. 92, no. 7, pp. 841–848, Jul. 2020, doi: 10.1002/jmv.25827.